Journal of
Materials Chemistry B

PAPER

View Article Online
View Journal | View Issue

Cite this: J. Mater. Chem. B, 2016, 4, 4585

Covalent functionalization and electrochemical tuning of reduced graphene oxide for the bioelectrocatalytic sensing of serum lactate†‡

Bhaskar Manna and C. Retna Raj*

Received 21st March 2016,
Accepted 31st May 2016

DOI: 10.1039/c6tb00721j

www.rsc.org/MaterialsB

Lactate is a byproduct of glycolysis and serum lactate can be used as a non-invasive biomarker in risk-stratifying patients with several life-threatening diseases. Herein, we describe the bioelectrocatalytic sensing of lactate using a covalently functionalized reduced graphene oxide (rGO)-based material. The development of a lactate biosensor involves the covalent functionalization of rGO with the *p*-nitrophenyl moiety, electrochemical generation of a surface-confined redox mediator and immobilization of L-lactate dehydrogenase (LDH). The covalently functionalized rGO was characterized by XRD, XPS, FTIR, Raman, resistivity and electrochemical measurements. The covalent attachment of the nitrophenyl moiety on the basal plane of the carbon network significantly influences the capacitive properties of rGO. The chemically functionalized rGO was electrochemically tuned to generate a redox mediator (rGO-PhNHOH). An electrochemically generated redox couple (PhNHOH/PhNO) exhibits reversible voltammetric response at ~ -0.06 V with a surface coverage of $(7.19 \pm 0.26) \times 10^{-9}$ mol cm^{-2}. The redox couple efficiently mediates the oxidation of NADH at 0.04 V, which is $\sim$600 mV less positive potential than the unmodified electrode. The electrode is highly sensitive towards NADH and it could detect as low as 0.4 μM NADH at the potential of 40 mV at neutral pH without any interference from co-existing bioanalytes. A lactate biosensor was developed using the rGO-PhNHOH functional material and lactate dehydrogenase. The surface-confined redox mediator could successfully detect the enzymatically generated NADH at 40 mV. The biosensor is highly sensitive (10.57 ± 0.38 nA μM^{-1} cm^{-2}) and shows linear response up to 90 μM of lactate. It could detect lactate as low as 2.5 μM without any interference from other analytes. This biosensor has been successfully used to quantify human serum lactate and the results are in excellent agreement with those obtained by the clinical method.

Introduction

Lactate, the key metabolite of anaerobic metabolism, is a potential biomarker for multiple sclerosis, malignancy in brain tumour, and cerebral ischemia.[1,2] The serum lactate level is an indirect marker of anaerobic glucose breakdown. The normal lactate level in human serum ranges from 3.21 to 6.68 mg dL^{-1}.[3] The precise quantification of serum lactate is important for the prevention and diagnosis of pathological disorders. The elevated level of serum lactate is an indication of multiple organ failure in adults[4] and it predicts the survival of children after open heart surgery.[5] The increase in the accumulation of lactate has been frequently observed in the malignant transformation of normal cells into the tumour cells.[6] The high level of lactate points out the possibility of metastases, patient survival and recurrence tumor. Hyperlactatemia and tissue hypoperfusion are shown to be a predictor of mortality.[7] The elevated level of serum lactate in surgical patients indicates that the patient is at risk.[7] The development of highly sensitive sensors for the detection and quantification of serum lactate is in demand in clinical diagnosis, biotechnology and sports medicine. Although several methods based on chromatography and spectrophotometry are available,[8–12] the analysis involves complex procedures. The amperometric method gained considerable interest in the biosensor industry as it does not require expensive equipment or tedious procedures. The amperometric biosensing of lactate requires either the enzyme lactate oxidase (LOx)[13–15] or lactate dehydrogenase (LDH).[16] The biosensing of lactate with LOx involves the quantification of enzymatically generated H_2O_2. The amount of H_2O_2 generated during the enzymatic reaction is proportional to the concentration of lactate present in the sample. The quantification of enzymatically

Functional Materials and Electrochemistry Laboratory, Department of Chemistry, Indian Institute of Technology, Kharagpur 721302, West Bengal, India.
E-mail: crraj@chem.iitkgp.ernet.in; Fax: +91 3222 282522

† Dedicated to Prof. R. Ramaraj on the occasion of his 60th birthday

‡ Electronic supplementary information (ESI) available. See DOI: 10.1039/c6tb00721j

produced H_2O_2 by electrochemical oxidation requires high overpotential and it invites interference due to other easily oxidizable analytes coexisting with lactate. On the other hand, amperometric biosensing of lactate with LDH involves the measurement of enzymatically generated NADH. The quantification of NADH by electrochemical oxidation requires suitable redox mediators, as the oxidation on unmodified electrodes requires high overpotential as large as +0.85 V (Ag/AgCl), though the formal potential of NAD/NADH at neutral pH is −0.560 V (SCE). The sluggish electron transfer kinetics and fouling of the electrode surface by adsorption of electrochemically generated intermediates actually cause high overpotential.[17] The high overpotential can be reduced using a suitable redox mediator.[18] Modification of an electrode with functional materials that are capable of promoting electron transfer and the use of redox mediators can decrease the overpotential for the oxidation of NADH.

Graphene, one of the allotropes of carbon, is a two dimensional honeycomb lattice. In recent years, graphene has emerged as one of the ideal materials for electrochemical applications because of its unique structural and electronic properties. Its high electrical conductivity, large surface area, good biocompatibility, and low manufacturing cost make it an excellent candidate for the development of electrochemical sensors/biosensors.[19,20] The extended π-conjugation of graphene makes it a highly electrical conductive material. Redox enzymes immobilized on graphene retain their enzymatic activity.[20–22] The covalent wiring of a potential redox mediator onto the carbon framework of reduced graphene oxide for amperometric biosensing application is a promising approach. Several approaches have been adopted in the past for the covalent wiring of the redox mediator.[23–25] Our group is interested in the development of amperometric biosensors based on functional materials and molecular assemblies.[26] The carbon framework that carries the redox mediator can provide an ideal environment for the redox enzyme. The high mechanical strength and electronic conductivity ensure fast response time, high stability and sensitivity. Herein, considering the importance of the development of a lactate biosensor, we demonstrate (i) the covalent wiring of *p*-nitroaniline onto the carbon network, (ii) electrochemical generation of a redox mediator capable of catalysing the oxidation of enzymatically generated NADH and (iii) the development of a LDH-based amperometric biosensor for the quantification of lactate in human serum.

Experimental section

Reagents and materials

Graphite, H_2O_2 (30%), Nafion® (5 wt% solution in lower alcohol), and L-lactate dehydrogenase (from rabbit muscle) were obtained from Sigma-Aldrich. $NaNO_2$ and *p*-nitroaniline were obtained from Merck. All other chemicals used in this investigation were of analytical grade (99.9%) and used without further purification. Phosphate buffer solutions (PBS, 0.1 M) of different pHs were used as supporting electrolytes in the voltammetric and amperometric measurements. All the solutions used in this investigation were prepared using Millipore water (Milli-Q-system).

Instrumentation

Fourier transform infrared spectroscopy (FTIR) measurements were performed using a Perkin-Elmer FTIR spectrophotometer RX1. Raman measurements were performed using a HORIBA JOBIN YVON (France, model no. T64000) equipped with a thermoelectric cooled CCD detector. The samples were excited with an air cooled argon–krypton mixed ion gas laser of wavelength 514.5 nm with a power of 120 mW. X-ray diffraction (XRD) analysis was carried out using a PANalytical high resolution X'pert PRO X-ray diffraction unit using Ni-filtered CuKα (λ = 1.54 Å). X-ray photoelectron spectroscopy (XPS) measurements were performed using a PHI 5000 VersaProbe II scanning XPS microprobe (ULVAC-PHI, inc.) using the energy source Al (Kα, $h\nu$ = 1486.6 eV). The spectra were analyzed using XPSPEAK 4.1 software, and AFM measurements were performed using Agilent Technologies 5500. Resistivity was measured by the van der Pauw four-probe method using an ECOPiA Hall measurement system (South Korea, model no. HMS-5300) attached to a sample holder (AHT 55T3) with a magnetic strength of 0.545 T. All the voltammetric and amperometric measurements were carried out using a CHI643B electrochemical analyzer attached to a current booster (CH Instruments, Austin, TX). A two-compartment three-electrode cell with glassy carbon (GC) working (0.07 cm^2), platinum wire auxiliary, and Ag/AgCl (3 M KCl) reference electrodes was used in the voltammetric and amperometric measurements. Cyclic charge–discharge experiments were performed using a Gamry Reference 3000 potentiostat/galvanostat at the current density of 0.2 Ag^{-1} in the potential window of −0.3 to 0.3 V (Ag/AgCl).

Synthesis of graphene oxide and reduced graphene oxide

Graphene oxide (GO) was synthesized from pristine graphite by modified Hummer's method.[27] Briefly, 25 mL of concentrated H_2SO_4 was slowly added to a mixture of graphite powder (0.5 g) and $NaNO_3$ (0.5 g) in a 500 mL round bottom (RB) flask at 0 °C. Solid $KMnO_4$ (3 g) was added to the RB flask at <5 °C and the mixture was stirred continuously for 1 h at room temperature. Water (150 mL) was slowly added to it and stirred for another 15 min. Then H_2O_2 solution (30%) was added to the RB flask until the gas evolution was ceased. The residue was then washed repeatedly with 15% HCl solution until the washing solution was free from sulfate ions (tested with $BaCl_2$ solution). The residue was further washed with Millipore water and dried in a vacuum to get the yellow-brown GO. The reduced graphene oxide (rGO) nanosheets were obtained from GO by its reduction using $NaBH_4$. Typically 100 mg of GO was dispersed in water (75 mL) by sonication for ~1 h. $NaBH_4$ (200 mg) was added to GO dispersion and it was stirred vigorously for 30 min, and then the resulting mixture was heated at 135 °C for 6 h. Black coloured rGO was obtained, and it was separated by centrifugation and washed repeatedly with Millipore water and dried in a vacuum. The dried product was ground using a mortar pestle and subjected to the functionalization and other measurements.

Covalent functionalization of rGO with the nitrophenyl moiety

rGO was covalently functionalised with the *p*-nitrophenyl moiety using *p*-nitroaniline according to the procedure adopted

for the synthesis of sulfonated graphene.[28] Typically, an ice-cold $NaNO_2$ solution (3 mg mL^{-1}) was added dropwise to a beaker containing ice-cold *p*-nitroaniline (5 mM) and HCl (10 mM) under constant stirring. The mixture was stirred for 10 min and then poured into rGO dispersion in Millipore water (20 mg per 10 mL) with stirring. The stirring was continued for another 2 h at room temperature and the mixture was centrifuged. The residue was thoroughly washed with Millipore water and ethanol to remove the physically adsorbed reactant, if any. The product (rGO-$PhNO_2$) was dried in a vacuum and used for further studies.

Electrochemical generation of a surface-confined redox mediator

GC electrodes (0.07 cm^2) were used as the substrate for making rGO-$PhNO_2$ film. Before modification, the electrodes were polished well with fine emery paper and alumina (0.05 μm) slurries and then sonicated in Millipore water for ~5 min. Finally the electrodes were thoroughly rinsed with Millipore water and used for modification. The rGO-$PhNO_2$ material (0.6 mg) was dispersed in 1 wt% ethanolic Nafion® solution (300 μL) by sonication and an aliquot of 20 μL of this dispersion was uniformly coated on the cleaned GC electrode and dried at room temperature for 30 min. The rGO-$PhNO_2$ modified GC electrode was then subjected to potential cycling between 0.2 and −0.6 V (7–8 cycles) to generate the surface-confined redox mediator, rGO-PhNHOH. After potential cycling the electrode was thoroughly washed with water and subjected to other experiments.

Preparation of an amperometric L-lactate biosensor

The rGO-$PhNO_2$ modified GC electrode was first subjected to potential cycling for the generation of the redox mediator, rGO-PhNHOH. Then the electrode was washed with Millipore water and dried in air for ~5 h. Then 10 μL of lactate dehydrogenase (LDH) (5.2 U μL^{-1}) in 5 mM PBS of pH 7.2 was uniformly coated on the electrode and dried at 4 °C for 6 h. The amperometric measurements of lactate were performed in a stirred 0.1 M PBS (pH 7.2) containing a required amount of NAD^+ using the LDH immobilized electrode. The electrode was polarised at the potential of 0.04 V and lactate was injected at regular intervals. All the measurements have been repeated at least for three times and the standard deviation of the repeated measurements was less than 5%.

Results and discussion

Covalent grafting of $PhNO_2$ and characterization of rGO-$PhNO_2$

The covalent grafting of $PhNO_2$ was achieved by the *in situ* diazotization of the amine precursor (H_2N–Ph-NO_2) under ice-cold conditions. The functionalization involves the *in situ* generation of the diazonium derivative and the covalent attachment of the –$PhNO_2$ functionality through a radical mechanism[29] (Scheme 1 and Fig. S1, ESI‡). The concentration of the precursor was optimized to achieve maximum grafting. The reaction of the

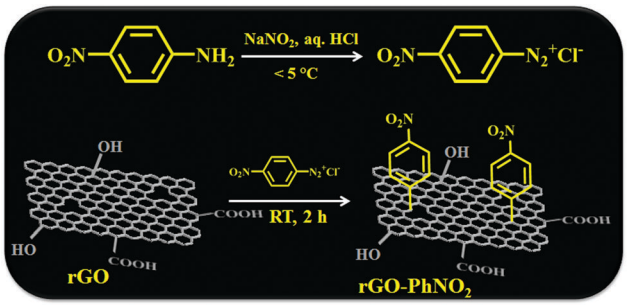

Scheme 1 Scheme illustrating the synthesis of rGO-$PhNO_2$.

in situ generated 4-nitrophenyl diazonium cation on the carbon network favours the covalent grafting of the –$PhNO_2$ moiety. It is generally accepted that the diazonium ions decompose in aqueous acidic solution in the presence of π electron systems.[29,30] In our case, the conjugated rGO sheet functions as a nucleophile and the phenyl radical generated reacts on the rGO surface.[31] The concerted decarboxylation[29] by the *in situ* generated arenium ion and the grafting of –$PhNO_2$ cannot be ruled out. The diazonium cation can replace the oxygen functionalities such as –COOH. The carbon centre attached to the unreduced carboxyl group on the edges of the rGO sheet can also be the sites for the grafting of –$PhNO_2$. We propose that the grafting of –$PhNO_2$ preferably occurs over the basal plane rather than the edges of the sheets (*vide supra*). The as-synthesized rGO and rGO-$PhNO_2$ were characterized using FTIR, XRD, XPS and AFM measurements. The FTIR spectrum of GO shows characteristic signatures for the oxygen containing functionalities such as –OH (3409 cm^{-1}), –C═O (1722 cm^{-1}), C═C (1617 cm^{-1}), epoxy symmetrical ring deformation vibration (1225 cm^{-1}), and alkoxy C–O (1051 cm^{-1}) (Fig. 1A). In the case of rGO, the intensity of these peaks has significantly decreased, and some of the peaks have vanished, due to the removal of oxygen functionalities of GO. The skeletal vibration of rGO appears at 1567 cm^{-1}. rGO-$PhNO_2$ shows characteristic peaks at 1520 ($\nu_{asym\,str}$ of N–O) and 1344 cm^{-1} ($\nu_{sym\,str}$ of N–O) for the nitro group, supporting the grafting of the $PhNO_2$ moiety onto the rGO sheets.

The Raman spectrum of GO shows the D and G bands at 1367 and 1608 cm^{-1}, respectively (Fig. S2, ESI‡). The chemical reduction of GO to rGO shifts both D and G bands to a lower wavenumber and the intensity ratio (I_D/I_G) of these bands increases from 0.61 to 0.77, implying that the reduction process alters the structural integrity of the honeycomb carbon network and generates plenty of defects[32] and the average size of the sp^2 domain upon reduction of the exfoliated GO decreases.[33,34] The I_D/I_G ratio further increases to 0.85 when rGO is functionalized with the *p*-nitrophenyl moiety. The increase in the I_D/I_G ratio suggests the increase in the disorder due to the covalent attachment of the *p*-nitrophenyl moiety on the rGO sheet. The XRD profile of GO shows characteristic diffraction at $2\theta = 9.88°$ corresponding to the (002) plane (Fig. 1B). After the reduction of GO to rGO, this diffraction shifted to $2\theta = 24.95°$. The removal of oxygen containing functional groups and restoration of π-conjugation actually shifts the diffraction to a higher angle.

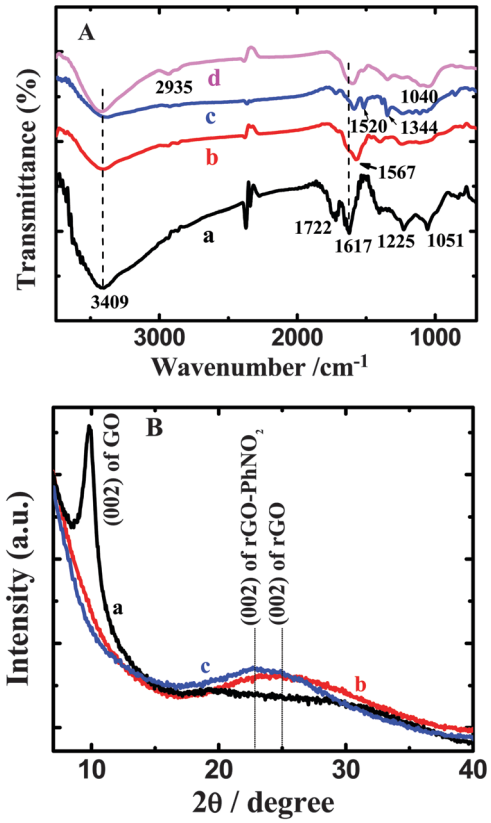

Fig. 1 (A) FTIR spectral profile of GO (a), rGO (b), rGO-$PhNO_2$ (c), and rGO-PhNHOH (d); (B) XRD profile of GO (a), rGO (b) and rGO-$PhNO_2$ (c).

Such a shift indicates the decrease in the interlayer distance. In the case of rGO-$PhNO_2$, the diffraction of the (002) plane shifted to a lower angle, implying that the covalent attachment of $-PhNO_2$ groups on the basal plane increases the interlayer distance; the interlayer distance increases from 0.356 to 0.388 nm. The height profile of the AFM image of rGO shows that the thickness of the sheet is 4–8 nm suggesting the aggregation of 3–6 layers of rGO (Fig. S3, ESI‡). In the case of rGO-$PhNO_2$ the height profile analysis shows spikes, suggesting the presence of bulky functional groups on rGO sheets.[35] The survey scan XPS profile of rGO-$PhNO_2$ shows signatures for C, O and N (Fig. 2) whereas the rGO profile shows signatures only for C and O (Fig. S4, ESI‡). The deconvulated C1s XPS profile of rGO (Fig. 2) shows peaks centered at 284.45 and 285.3 eV corresponding to the binding energy of C=C/C–C and sp^3C, respectively.[36] The other less intense peaks at the binding energy of 286.44, 287.9 and 288.9 eV can be ascribed to C–O, C=O and O–C=O functionalities, respectively.[36] In the case of rGO-$PhNO_2$ (Fig. 2), the peaks are rather broad with respect to the unfunctionalized rGO. The covalent functionalization of rGO is known to exhibit such broadening for the C1s signal.[37] A new peak at 285.8 eV corresponding to C–N was observed. The band observed at 283.6 eV can be ascribed to the p-type doping of rGO.[38] The functionalization of rGO with $-PhNO_2$ actually increases the percentage of sp^3 carbon; an ~10% increase in sp^3 carbon was noticed after functionalization. The peaks centered at 284.4, 285.4, 286.4, 287.9 and 288.9 eV correspond to C=C/C–C, sp^3C, C–O, C=O and O–C=O, respectively. The N1s spectrum of rGO-$PhNO_2$ (Fig. 2) shows two peaks centered at 399.90 and 408.44 eV. The peak at 408.44 eV corresponds to the nitro group on the rGO sheets whereas the peak at 399.90 eV is ascribed to the reduced nitrogen species generated during the XPS measurement.[38] The weight percentage of $PhNO_2$ attached to the rGO network was obtained from XPS measurement using the N1s signal. The weight percentage was calculated to be 9.11.

Cyclic voltammetry is one of the ideal techniques to characterize the rGO-based materials. The capacitance of GO and rGO-based materials is highly sensitive to the electronic environment. GO is known to be an insulator and the capacitance is significantly less owing to the loss of conjugation during oxidative exfoliation. The careful examination of the non-faradic voltammetric profile (Fig. 3) shows that rGO has the highest capacitance. This is in accordance with the electronic nature of rGO. The large surface area and high electronic conductivity due to extended conjugation of the carbon network yield large capacitance. On the other hand, the capacitance of rGO-$PhNO_2$ is much less than rGO and slightly higher than GO. The capacitance values of GO, rGO, and rGO-$PhNO_2$ follow the order GO < rGO-$PhNO_2$ < rGO. It should be noted here that the covalent functionalization of rGO with $PhNO_2$ actually removes the extended π conjugation of the carbon network, resulting in a decrease in the capacitance. This further confirms the covalent functionalization of the $-PhNO_2$ group on the carbon skeleton. To further understand the influence of the functionalization of rGO sheets with $-PhNO_2$ on the electrical properties, conductivity measurement was performed using the four-probe method. As anticipated rGO has highest electrical conductivity and it significantly decreases upon functionalization with $-PhNO_2$. The electrical conductivity follows the order GO (1.16×10^{-6} S cm^{-1}) < rGO-$PhNO_2$ (8.93×10^{-5} S cm^{-1}) < rGO (1.68×10^{-3} S cm^{-1}), supporting the significant influence of the covalent functionalization of rGO. The decrease in the electrical conductivity and capacitance implies that the covalent attachment of $-PhNO_2$ actually occurs at the basal plane of rGO. It should be noted here that the electrical conductivity of rGO-$PhNO_2$ is higher than GO and it can serve as a suitable matrix for enzyme immobilization.

Electrochemical generation of a surface-confined redox mediator

The covalently attached $-PhNO_2$ moiety on the rGO surface was further electrochemically converted to a redox mediator, PhNHOH. The electrode modified with rGO-$PhNO_2$ was subjected to potential cycling in an optimized potential window of 0.2 V to −0.6 V in PBS of pH 7.2. As shown in Fig. 4a, a large cathodic wave at ~−0.6 V was noticed while sweeping the potential from 0.2 V. A gradual decrease in the magnitude of the cathodic wave associated with the appearance of a new symmetric redox peak at ~−0.06 V was observed in the subsequent sweeps. The reversible peak attained the maximum current within 7–8 potential cycles. The cathodic wave obtained at ~−0.6 V can be ascribed to the conversion of the surface-confined nitrophenyl moiety of

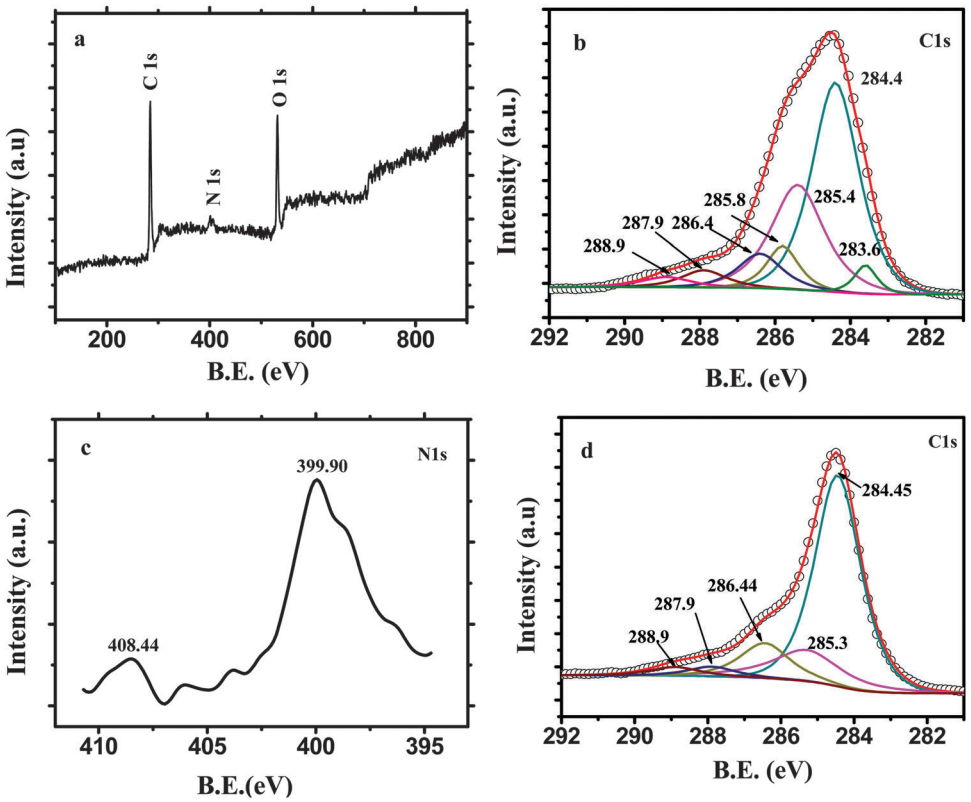

Fig. 2 Survey scan (a) and deconvoluted C1s (b) and N1s (c) XPS profiles of rGO-$PhNO_2$. The deconvoluted C1s profile of rGO is shown in (d).

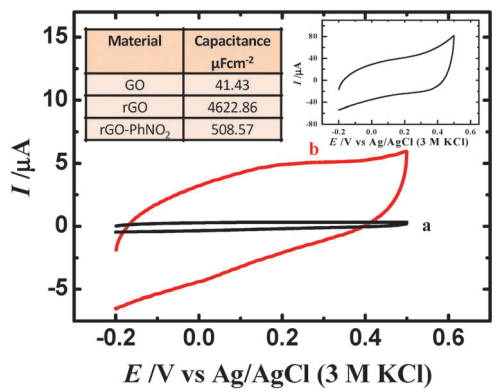

Fig. 3 Cyclic voltammetric responses of GO (a), rGO-$PhNO_2$ (b) and rGO (inset) modified GC electrodes in 0.1 M PBS (pH 7.2). Scan rate: 0.1 V s^{-1}.

the carbon network to phenylhydroxylamine (Scheme 2). The electrochemical reduction of $PhNO_2$ is known to generate various products, depending on the solvent, solution pH and the potential window.[39] Aminophenol and aniline are the predominant products in protic solvent and phenylhydroxylamine is the intermediate species.[40] In our case, as the –$PhNO_2$ moiety is covalently grafted on the rGO sheet, the generation of aminophenol is completely ruled out. The generation of surface-confined aniline can be controlled by controlling the potential window. The surface confined –$PhNO_2$ initially undergoes four electron reduction generating –PhNHOH which can undergo reversible electron transfer to produce –PhNO. The redox couple, PhNO/PhNHOH, can be selectively generated by controlling the cathodic potential window. The reversible redox peak obtained at ~−0.06 V corresponds to the redox reaction of the PhNO/PhNHOH redox couple (Fig. 4b). The peak-to-peak separation was found to be ~130 mV and does not change appreciably with the sweep rate. The redox peak is rather broad at high sweep rates (Fig. S5, ESI‡). The peak current linearly scales with the sweep rate, indicating that the redox response is due to the surface-confined redox species. The loading of rGO-$PhNO_2$ on the electrode surface has a significant influence on the surface coverage of the mediator and maximum surface coverage was obtained at the loading of 0.57 mg cm^{-2}. The surface coverage of the redox couple was obtained by integrating the anodic/cathodic peak and was (7.19 ± 0.26) × 10^{-9} mol cm^{-2}. The influence of pH on the redox response was examined in the supporting electrolyte of various pH values (Fig. S6, ESI‡). The peak potential shifts by 49 mV per unit pH. The value is slightly less than that which is expected for a redox reaction involving electrons and protons in the 1 : 1 ratio. The heterogeneous electron transfer rate constant (k_s) was calculated to be 1.97 s^{-1} using the Laviron approach.[41] The electrochemically generated rGO-PhNHOH shows new peaks at 2935 and 1040 cm^{-1} corresponding to the stretching vibration of N–H and N–O bonds of the –NHOH moiety. Moreover, an observable increase in the peak intensity at 3409 cm^{-1} due to the presence of PhNHOH groups was noticed (Fig. 1A). In order to examine the capacitive performance of the modified electrode after the electrogeneration of the redox mediator, galvanostatic charge–discharge experiments

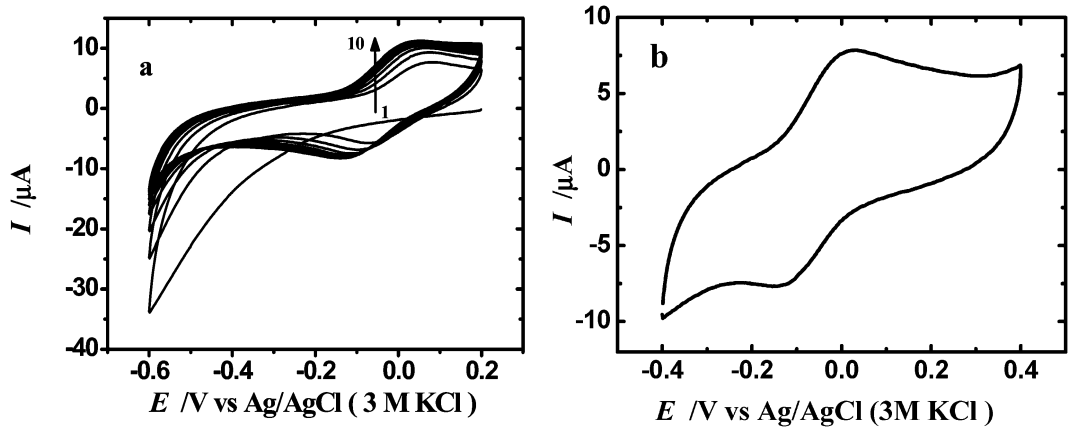

Fig. 4 (a) Electrochemical generation of the surface-confined redox couple (PhNHOH/PhNO). The potential of the rGO-$PhNO_2$ electrode was cycled between 0.2 V and −0.6 V in 0.1 M PBS (pH 7) for 10 consecutive cycles. Scan rate: 0.01 V s^{-1}. (b) Cyclic voltammograms of the electrochemically generated surface-confined redox mediator in 0.1 M PBS (pH 7) at a scan rate of 0.01 V s^{-1}.

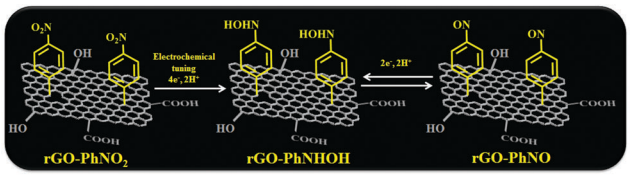

Scheme 2 Scheme illustrating the electrochemical tuning of chemically functionalized rGO.

have been performed. The specific capacitance of the rGO-PhNHOH electrode (1.03 Fg^{-1}) is slightly higher than the parent rGO-$PhNO_2$ (0.76 Fg^{-1}). However, it is significantly lower than the as-synthesized rGO (10.23 Fg^{-1}). The slight enhancement of the specific capacitance of rGO-PhNHOH can be attributed to the pseudocapacitive contribution originating from the redox mediator.

Electrocatalytic sensing of NADH

The main objective of the present work is to develop a dehydrogenase-based amperometric biosensor for the lactate biomarker. As the function of a dehydrogenase-based biosensor depends on the enzymatically generated NADH, first we have investigated electrocatalytic oxidation of NADH. As the redox reaction of our electrogenerated redox mediator rGO-PhNHOH involves $2e^-$ and $2H^+$ and redox potential falls in the potential region where NADH can be efficiently oxidized, we have examined its catalytic response towards oxidation of NADH. Fig. 5A illustrates the electrocatalytic response of rGO-PhNHOH toward NADH. As shown in the figure, the oxidation peak increases at the potential of 40 mV in the presence of NADH. The enhancement of the anodic peak associated with a decrease in the cathodic peak in the presence of NADH indicates the electrocatalytic effect of the surface-confined mediator. No characteristic oxidation peak was obtained on the rGO modified GC electrode, though enhancement in the current was noticed in the potential region of 0.1 to 0.4 V (Fig. S7, ESI‡). On the unmodified GC, the oxidation actually occurs at a more positive potential (>600 mV). A significant (200–600 mV) decrease in the overpotential for NADH oxidation with respect to the unmodified GC and rGO/GC electrodes has been achieved with rGO-PhNHOH. The electrocatalytic current on the modified electrode depends on the surface coverage of the electrogenerated redox mediator and maximum electrocatalytic current was obtained at the surface

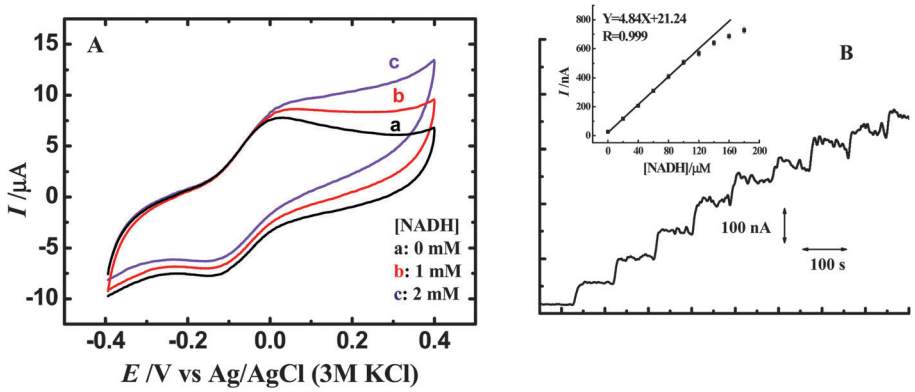

Fig. 5 (A) Electrochemical responses of the rGO-PhNHOH/GC electrode in the presence and absence of NADH. Scan rate: 10 mV s^{-1}. (B) Amperometric *i*–*t* curve for the oxidation of NADH at the rGO-PhNHOH modified electrode polarised at 0.04 V in a stirred solution of 0.1 M PBS (pH 7.2). Each addition increased the concentration of NADH by 20 μM. The inset shows the corresponding calibration plot.

coverage of (7.19 ± 0.26) × 10^{-9} mol cm^{-2}. The amperometric measurement of NADH oxidation was performed in a stirred 0.1 M PBS (pH 7.2), and NADH was injected at regular intervals. Fig. 5B shows amperometric response obtained for the NADH oxidation on the rGO-PhNHOH modified electrode at 0.04 V. The sensitivity was obtained from the calibration plot and was 69.14 ± 0.90 nA μM^{-1} cm^{-2}. The electrode has linear response up to 100 μM with a response time of 21 s. This electrode could detect as low as 0.4 μM NADH (S/N = 6) at the potential of 0.04 V at neutral pH. It should be mentioned here that no such response was obtained with GC or rGO/GC electrodes at 0.04 V, confirming that the amperometric current obtained is actually due to the mediated oxidation of NADH by the redox couple (–NHOH/–NO) covalently linked with rGO. The excellent analytical performance of the electrode is due to the improved electronic transport and effective mediation by the redox couple (–NO/–NHOH). The electrode is highly stable and the amperometric response does not change significantly with time. The operational stability of the electrode was investigated polarizing the electrode at 0.04 V and injecting 100 μM NADH (Fig. S8, ESI‡). No significant change in the current was observed for a long time. The co-existing common easily oxidisable analytes such as ascorbic acid and uric acid in the biological fluids can interfere with the biosensing of lactate. Amperometric sensing of NADH in the presence of large excess of interfering ascorbate and urate was performed. Aliquots of ascorbate and urate (0.1 mM each) were injected polarizing the electrode at 0.04 V. The addition of the interfering ascorbate/urate does not alter the amperometric current for the oxidation of NADH (Fig. S9, ESI‡), indicating that both ascorbate and urate do not interfere the amperometric measurement of NADH. Although the oxidation of NADH as well as ascorbate and urate involves $2e^-$, the mediator modified electrode could selectively oxidize NADH.

Amperometric biosensing of lactate

Amperometric biosensing of lactate was achieved according to the enzymatic reaction illustrated in Fig. 6. The amperometric sensing of lactate involves the quantification of enzymatically generated NADH at 0.04 V, using the surface-confined redox mediator. Fast and stable amperometric response was obtained upon repeated injection of lactate. No response was obtained in the absence of NAD^+ or lactate, confirming that the amperometric response is due to the oxidation of enzymatically generated NADH. The amperometric current is directly proportional to the concentration of lactate present in the sample. The amperometric response was linear up to 90 μM of lactate, and the sensitivity and response time of the biosensor were 10.57 ± 0.38 nA μM^{-1} cm^{-2} and 23 s, respectively. This electrode could detect as low as 2.5 μM L-lactate (S/N = 5) at the potential of 0.04 V in neutral pH. The amperometric response of the biosensor depends on the concentration of the cofactor of the enzyme. The effect of cofactor-concentration was investigated by varying the concentration with a constant amount of enzyme on the electrode surface and lactate in the test solution. The amperometric response increases with the

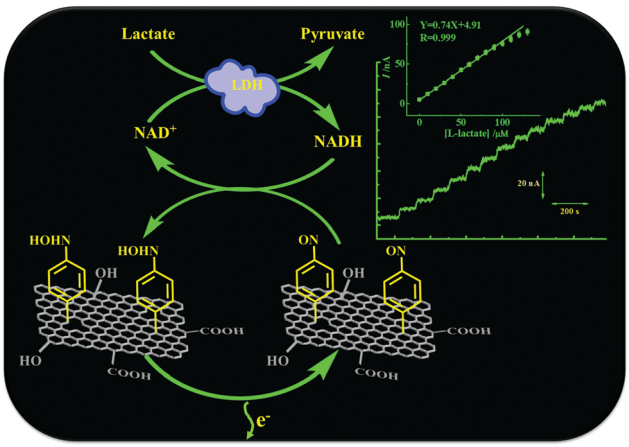

Fig. 6 Schematic illustration of the bioelectrocatalytic sensing of lactate and the corresponding amperometric response obtained at 0.04 V in a stirred solution of 0.1 M PBS (pH 7.2) containing 4 mM NAD^+. Each addition increased the concentration of lactate by 10 μM. The calibration plot is shown in the inset of the amperometric response.

increase in cofactor concentration and maximum response was obtained at 4 mM concentration of cofactor. A further increase in the concentration of NAD^+ leads to a decrease in the amperometric response, presumably due to the inhibitory effect (Fig. S10, ESI‡).

The apparent Michaelis–Menten constant (K_M^{app}) for lactate was calculated using a Lineweaver–Burk plot according to the following equation:

$$\frac{1}{I} = \frac{1}{I_{max}} + \frac{K_M^{app}}{I_{max}[S]}$$

where I is the steady state current, I_{max} is the maximum current obtained at the saturated level of L-lactate and [S] is the concentration of lactate. The graphical analysis of the plot provides the K_M^{app} = 86 μM and I_{max} = 115.47 nA for L-lactate. The K_M^{app} value is strongly dependent on the immobilization matrix. The lower value of K_M^{app} obtained here implies the strong affinity of the substrate to the enzyme which facilitates the enzymatic reaction.[42,43] The performance of our sensor in terms of detection potential is superior to the existing lactate biosensors[44–57] (Table S1, ESI‡). Interestingly, our sensor could operate at the potential of 0.04 V without any interference from the coexisting analytes. Although several lactate biosensors have been reported in the literature, in most of the cases the practical utility is not fully demonstrated.[45–51,53–57] Practical application of the biosensor was examined using three human serum samples collected from B. C. Roy Technology Hospital, IIT Kharagpur. The undiluted serum samples were injected into the supporting electrolyte solution and amperometric repose was monitored to quantify the amount of lactate in each sample. Three independent measurements have been performed with each samples and the relative standard deviation is less than 5% in all the cases (Table 1). To validate the performance of our biosensor, the amount of lactate was quantified by the conventional clinical procedures. Interestingly, the concentrations of lactate quantified using our biosensor is in close agreement with those obtained by the clinical method (Table 1), authenticating the

Table 1 Biosensing of L-lactate in human serum samples

Sample no.	Measured with our biosensor[a] (mg dL^{-1})	Measured by the clinical method (mg dL^{-1})	RSD[b] (%)
1	12.94	12.88	4.79
2	14.46	14.51	3.94
3	13.49	13.66	3.26

[a] Average of three independent measurements. [b] RSD: obtained from three independent measurements of each sample.

validity of the measurement. As the fabrication procedure is rather simple and it has excellent performance towards real sample, our biosensor has high potential for the quantification of the biomarker.

Conclusions

The covalent functionalization of rGO with the $-PhNO_2$ moiety and electrogeneration of the redox couple rGO-PhNHOH/PhNO for the biosensing of the lactate biomarker are established. rGO-$PhNO_2$ was electrochemically tuned to obtain a surface-confined reversible redox couple. It has high surface coverage and it undergoes a facile electron transfer reaction. The surface-confined redox couple efficiently mediates the oxidation of NADH at the potential of 0.04 V, which is $\sim$600 mV less positive than the unmodified electrode. Electrocatalytic sensing of NADH at the potential of 0.04 V without any interference from co-existing analytes is achieved. The dehydrogenase-based biosensor for the detection of the biomarker, lactate, is demonstrated. The practical application of the biosensor is demonstrated with human serum samples and the results are in close agreement with those obtained by the clinical method. The biosensor is highly sensitive, selective and shows rapid response towards the analyte. Our study demonstrates that the electrochemically tuned rGO platform is an ideal matrix for the immobilization of the redox enzyme and for the development of amperometric biosensors. The rGO-PhNHOH/LDH biosensor can be used for the amperometric sensing of the serum biomarker without any interference.

Acknowledgements

This work was supported by grants from Department of Science and Technology (DST) and Council of Scientific and Industrial Research (CSIR), New Delhi, and Indian Institute of Technology, Kharagpur. The authors are thankful to B. C. Roy Technology Hospital, IIT Kharagpur for providing human serum samples.

References

1 A. M. Amorini, V. Nociti, A. Petzold, C. Gasperini, E. Quartuccio, G. Lazzarino, V. D. Pietro, A. Belli, S. Signoretti, R. Vagnozzi, G. Lazzarino and B. Tavazzi, *Biochim. Biophys. Acta*, 2014, **1842**, 1137–1143.
2 K. K. Jain, *The Handbook of Biomarkers*, Humana Press, New York, 2010.
3 S. D'Auria, Z. Gryczynski, I. Gryczynski, M. Rossi and J. R. Lakowicz, *Anal. Biochem.*, 2000, **283**, 83–88.
4 J. Bakker, P. Gris, M. Coffernils, R. J. Kahn and J.-L. Vincent, *Am. J. Surg.*, 1996, **171**, 221–226.
5 L. B. Siegel, H. J. Dalton, J. H. Hertzog, R. A. Hopkins, R. L. Hannan and G. J. Hauser, *Intensive Care Med.*, 1996, **22**, 1418–1423.
6 F. Hirschhaeuser, U. G. A. Sattler and W. Mueller-Klieser, *Cancer Res.*, 2011, **71**, 6921–6925.
7 S. Walenta, M. Wetterling, M. Lehrke, G. Schwickert, K. Sundfør, E. K. Rofstad and W. Mueller-Klieser, *Cancer Res.*, 2000, **60**, 916–921.
8 B. Kannan, S. Jahanshahi-Anbuhi, R. H. Pelton, Y. Li, C. D. M. Filipe and J. D. Brennan, *Anal. Chem.*, 2015, **87**, 9288–9293.
9 D. B. M. Groegel, M. Link, A. Duerkop and O. S. Wolfbeis, *ChemBioChem*, 2011, **12**, 2779–2785.
10 D. Lafrance, L. C. Lands and D. H. Burns, *Talanta*, 2003, **60**, 635–641.
11 L. Fernandes, A. M. Relva, M. D. R. G. da Silva and A. M. C. Freitas, *J. Chromatogr. A*, 2003, **995**, 161–169.
12 R. W. Wulkan, R. Verwers, M. Neele and M. J. Mantel, *Ann. Clin. Biochem.*, 2001, **38**, 554–558.
13 J. M. Goran, J. L. Lyon and K. J. Stevenson, *Anal. Chem.*, 2011, **83**, 8123–8129.
14 M. Briones, E. Casero, M. D. Petit-Domínguez, M. A. Ruiz, A. M. Parra-Alfambra, F. Pariente, E. Lorenzo and L. Vázquez, *Biosens. Bioelectron.*, 2015, **68**, 521–528.
15 M. M. Pribil, G. U. Laptev, E. E. Karyakina and A. A. Karyakin, *Anal. Chem.*, 2014, **86**, 5215–5219.
16 Y. Lin, P. Yu, J. Hao, Y. Wang, T. Ohsaka and L. Mao, *Anal. Chem.*, 2014, **86**, 3895–3901.
17 J. Moiroux and P. J. Elving, *Anal. Chem.*, 1978, **50**, 1056–1062.
18 L. Gorton and E. Dominguez, Electrochemistry of NAD(P)+/NAD(P)H, in *Encyclopedia of Electrochemistry, (Bioelectrochemistry)*, ed. G. S. Wilson, Wiley-VCH, Weinheim, 2002, vol. 9, pp. 67–143.
19 M. J. Allen, V. C. Tung and R. B. Kaner, *Chem. Rev.*, 2010, **110**, 132–145.
20 C. Shan, H. Yang, J. Song, D. Han, A. Ivaska and L. Niu, *Anal. Chem.*, 2009, **81**, 2378–2382.
21 X. Zuo, S. He, D. Li, C. Peng, Q. Huang, S. Song and C. Fan, *Langmuir*, 2010, **26**, 1936–1939.
22 X. Kang, J. Wang, H. Wu, I. A. Aksay, J. Liu and Y. Lin, *Biosens. and Bioelectron.*, 2009, **25**, 901–905.
23 R. S. Dey and C. R. Raj, *ACS Appl. Mater. Interfaces*, 2013, **5**, 4791–4798.
24 V. Georgakilas, A. B. Bourlinos, R. Zboril, T. A. Steriotis, P. Dallas, A. K. Stubos and C. Trapalis, *Chem. Commun.*, 2010, **46**, 1766–1768.
25 Z. Liu, H. Zhou, Z. Huang, W. Wang, F. Zeng and Y. Kuang, *J. Mater. Chem. A*, 2013, **1**, 3454–3462.
26 R. S. Dey, R. K. Bera and C. R. Raj, *Anal. Bioanal. Chem.*, 2013, **405**, 3431–3448 and the references cited therein.
27 W. S. Hummers and R. E. Offeman, *J. Am. Chem. Soc.*, 1958, **80**, 1339.

28 Y. Si and E. T. Samulski, *Nano Lett.*, 2008, **8**, 1679–1682.
29 M. Toupin and D. Bélanger, *Langmuir*, 2008, **24**, 1910–1917.
30 H. Zollinger, *Acc. Chem. Res.*, 1973, **6**, 335–341.
31 J. L. Bahr, J. Yang, D. V. Kosynkin, M. J. Bronikowski, R. E. Smalley and J. M. Tour, *J. Am. Chem. Soc.*, 2001, **123**, 6536–6542.
32 I. K. Moon, J. Lee, R. S. Ruoff and H. Lee, *Nat. Commun.*, 2010, **1**, 73.
33 Y. Xu, H. Bai, G. Lu, C. Li and G. Shi, *J. Am. Chem. Soc.*, 2008, **130**, 5856–5857.
34 S. Stankovich, D. A. Dikin, R. D. Piner, K. A. Kohlhaas, A. Kleinhammes, Y. Jia, Y. Wu, S. T. Nguyen and R. S. Ruoff, *Carbon*, 2007, **45**, 1558–1565.
35 Y. Zhang, L. Ren, S. Wang, A. Marathe, J. Chaudhuri and G. Li, *J. Mater. Chem.*, 2011, **21**, 5386–5391.
36 W. Chen, L. Yan and P. R. Bangal, *J. Phys. Chem. C*, 2010, **114**, 19885–19890.
37 A. Sinitskii, A. Dimiev, D. A. Corley, A. A. Fursina, D. V. Kosynkin and J. M. Tour, *ACS Nano*, 2010, **4**, 1949–1954.
38 E. Bekyarova, M. E. Itkis, P. Ramesh, C. Berger, M. Sprinkle, W. A. de Heer and R. C. Haddon, *J. Am. Chem. Soc.*, 2009, **131**, 1336–1337.
39 D. S. Silvester, A. J. Wain, L. Aldous, C. Hardacre and R. G. Compton, *J. Electroanal. Chem.*, 2006, **596**, 131–140.
40 A. Cyr, P. Huot, G. Belot and J. Lessard, *Electrochim. Acta*, 1990, **35**, 147–152.
41 E. Laviron, *J. Electroanal. Chem.*, 1979, **101**, 19–28.
42 R. C. H. Kwan, P. Y. T. Hon, K. K. W. Mak and R. Renneberg, *Biosens. Bioelectron.*, 2004, **19**, 1745–1752.
43 R. S. Dey and C. R. Raj, *J. Phys. Chem. C*, 2010, **114**, 21427–21433.
44 M. M. Rahman, M. J. A. Shiddiky, M. A. Rahman and Y.-B. Shim, *Anal. Biochem.*, 2009, **384**, 159–165.
45 S. Pérez, S. Sánchez and E. Fbregas, *Electroanalysis*, 2012, **24**, 967–974.
46 A. Radoi, D. Compagnone, M. A. Valcarcel, P. Placidi, S. Materazzi, D. Moscone and G. Palleschi, *Electrochim. Acta*, 2008, **53**, 2161–2169.
47 H. Teymourian, A. Salimi and R. Hallaj, *Biosens. Bioelectron.*, 2012, **33**, 60–68.
48 A. Radoi, A. C. Obreja, S. A. V. Eremia, A. Bragaru, A. Dinescu and G.-L. Radu, *J. Appl. Electrochem.*, 2013, **43**, 985–994.
49 A. C. Pereira, M. R. Aguiar, A. Kisner, D. V. Macedo and L. T. Kubota, *Sens. Actuators, B*, 2007, **124**, 269–276.
50 F. Gao, X. Guo, J. Yin, D. Zhao, M. Li and L. Wang, *RSC Adv.*, 2011, **1**, 1301–1309.
51 B. Prieto-Simon, E. Fabregas and A. Hart, *Biosens. Bioelectron.*, 2007, **22**, 2663–2668.
52 S. Azzouzi, L. Rotariu, A. M. Benito, W. K. Maser, M. B. Ali and C. Bala, *Biosens. Bioelectron.*, 2015, **69**, 280–286.
53 Y.-C. Tsai, S.-Y. Chen and H.-W. Liaw, *Sens. Actuators, B*, 2007, **125**, 474–481.
54 M. Piano, S. Serban, R. Pittson, G. A. Drago and J. P. Hart, *Talanta*, 2010, **82**, 34–37.
55 J. Di, J. Cheng, Q. Xu, H. Zheng, J. Zhuang, Y. Sun, K. Wang, X. Mo and S. Bi, *Biosens. Bioelectron.*, 2007, **23**, 682–687.
56 N. Nesakumar, S. Sethuraman, U. M. Krishnan and J. B. B. Rayappan, *J. Colloid Interface Sci.*, 2013, **410**, 158–164.
57 N. Nesakumar, K. Thandavan, S. Sethuraman, U. M. Krishnan and J. B. B. Rayappan, *J. Colloid Interface Sci.*, 2014, **414**, 90–96.